Proceedings of the 16th European VLBI Network Symposium
Ros, E., Benke, P., Dzib, S., Rottmann, I., & Zensus, J.A. (eds.)
September 2nd-6th 2024, Bonn, Germany

Multi-wavelength-messenger study of Gamma Ray Bursts

G. Ghirlanda

INAF-Osservatorio Astronomico di Brera, Via E. Bianchi 46, I-23807 Merate (LC), Italy

Abstract. The potential of high-resolution VLBI radio observations in advancing our understanding of gamma-ray bursts (GRBs) and their afterglows is summarized. A couple of science cases are discussed in relation the VLBI observations of GRB 221009A and GRB 190829A. The unique capability of VLBI to resolve the size expansion of GRB 221009A revealed a superluminal expansion rate with an apparent speed of about $\beta = 1.6$ and a possible frequency dependent expansion rate which highlights the contribution of the forward and reverse shock emissions. In GRB 190829A, detected also at TeV energies, the VLBI source size constraints help to estimate magnetic field strength and electron acceleration efficiency, indicating that fewer than 1% of electrons reach non-thermal energies at the shock front. These findings underscore VLBI role in probing GRB afterglows within a multi-wavelength and multi-messenger framework.

1. Introduction

Gamma Ray Bursts (GRBs) are the most powerful explosive transients in the Universe. They have been detected up to z=9.2 (Cucchiara et al. 2011) and their typical luminosity, assuming isotropic emission, is in the range 10^{51-54} erg s^{-1} and their observed duration span almost four orders of magnitudes with the shortest spikes lasting <0.1 sec. GRBs signpost the death of massive stars ending their lifes as powerful "hypernovae" or as mergers of compact objects (at least one being a neutron star) in binaries. These two progenitor channels account for the broad division in short and long GRBs and for their observed properties (e.g. see Berger 2014). The short GRBs' compact merger origin has been spectacularly demonstrated by the event 170817 from which both a gravitational wave signal and a short GRB were captured (Abbott et al. 2017).

The electromagnetic emission of GRBs, typically named prompt and afterglow with reference, respectively, to the short high–energy and the long-lived pan-chromatic signals, originate from a collimated ultra relativistic jet. The prompt emission is due to internal dissipation while the afterglow is produced by the jet expansion and deceleration within the circum-burst medium. Therefore, the properties of the afterglow emission depend on intrinsic (e.g. jet energy and its angular distribution within the jet) and extrinsic (e.g. jet orientation, density of the interstellar medium where it propagates) factors.

Radio observations have the unique power to couple high sensitivity with great imagining capabilities. VLBI observations of GRBs provided, in a handful of cases, direct measurements of the temporal growth of the size of the afterglow owing to the relativistic expansion of a jet observed close to its axis (GRB 230329 - Taylor et al. 2004 - and GRB 221009A - Giarratana et al. (2024)) or the measurement of the displacement of the source centroid due to a considerably off-axis orientation of the line of sight (GRB 170817 - Mooley et al. 2018; Ghirlanda et al. 2019).

The modelling of the multi-wavelength afterglow emission jointly with size and/or proper motion measurements or constraints alleviate the issue of afterglow model parameter degeneracy, which in most GRB prevents the determination of the source physical properties.

2. Radio observations of GRBs

Figure 1 (left panel) shows a collection of radio lightcurves of GRBs (blue symbols) from Laskar et al. (2023) in the radio luminosity versus time plot. GRBs are among the most luminous transients compared, for instance, with supernovae, relativistic SNe and Tidal Disruption Events (light, dark grey and green symbols in Fig. 1 - left panel). While the X-ray light curves of GRBs (right panel of Fig. 1) are typically monotonically decreasing in time and detected from the earliest epochs up to a few months, radio emission is still detected, in a number of cases, up to a few years after and it displays an overall "bumpy" shape with several curves rising at very early times. This is due to the fact that the early afterglow emission is self absorbed at radio frequencies and becomes brighter as the jet expands and becomes transparent to synchrotron self-absorption. The relatively slow evolution of the radio afterglow emission may have contributed to relatively small detection rate of radio emission (Chandra & Frail (2012)) at the beginning of the afterglow era, just after the launch of the Swift satellite (Gehrels et al. 2004), owing to the limited efforts to search for the radio emission with repeated observations (Ghirlanda et al. (2013)).

The afterglow of GRBs is due to synchrotron self Compton emission by relativistic electrons accelerated in relativistic collision–less shocks. As the jet expands into its sorrounding medium it decelerates and develops two shocks develop around the contact discontinuity, namely the forward and reverse shock (FS and RS, hereafter). While the FS accelerates particles and increases, via turbolence, the low magnetic field of the interstellar medium,

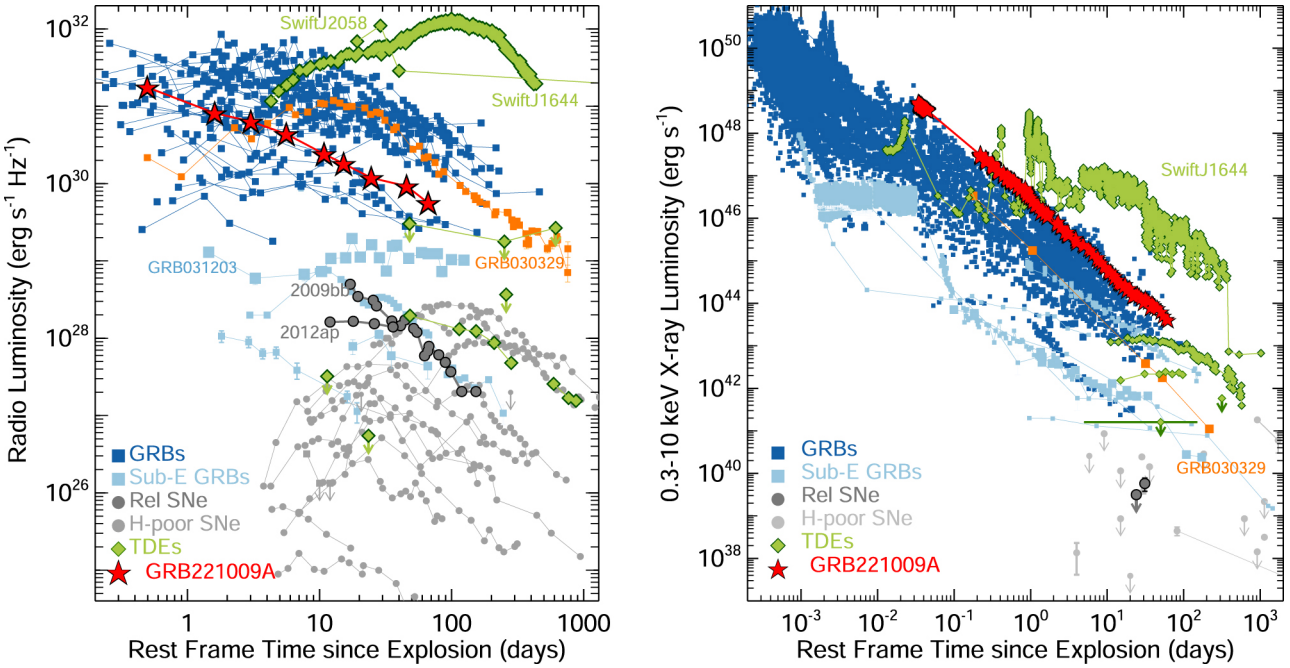

Fig. 1: Left: radio spectral luminosity (8 GHz - rest frame) as a function of rest-frame time for GRBs (blue). Two notable cases are highlighted (GRB 221009A and GRB 030329, red and orange symbols). Comparison with SN (grey) and TDE (green). Right: X-ray luminosity (0.3–10 keV band). Figure from Laskar et al. (2023)

the RS acts on the same material of the jet. Indeed, owing to relative small velocity constrast between the RS and the jet, the RS is, compared to the FS, relatively less efficient in accelerating electrons to very large energies and its duration is limited by the time jet spends to pass through the shock discontinuity. Therefore, the RS contribution dominating the early afterglow emission in the radio band. The RS luminosity depends on several parameters, most notably the shock duration, the jet initial Lorentz factor and the jet magnetisation.

Two notable examples where a clear signature of the RS emission has been detected in the radio band are GRB 130427A (Perley et al. 2014) and GRB 221009A (e.g. Bright et al. 2023). In the latter case, the rapid follow up capabilities of the Arcminutes MicroKelivin Imager Large Array (AMI-LA) and Allen Telescope Array (ATA) from 3 to 15 Ghz starting as early as 3hrs after the burst showed a flux increase as $t^{1.32}$ accompained by a clear spectral evolution from a thick ($\nu^{2.5}$) to a thin (ν^{0}) emission regime (see e.g. Fig.2 in Bright et al. 2023). Such flux and frequency time evolution is consistent with being produced by RS emission.

3. Radio imaging of GRB jet emission

The unique contribution of radio observations to unveil the jet physics and properties consists in exploiting the high resolution acheivable with VLBI observations.

The exceptionally bright gamma-ray burst GRB 221009A was observed with the European VLBI Network (EVN) between 40 and 262 days post-explosion by Giarratana et al. (2024). Observations detected a projected size of 0.39 mas at 52 days, expanding to 0.80 mas by day 252. These observations enabled tracking, for the second ever GRB, of the projected shock-wave size with unprecedented accuracy (see Fig.2), revealing a size expansion $\propto t^{0.69}$ corresponding to an apparent expansion velocity of about $\beta_{\rm app} = 1.6$, consistent with the highly relativistic motion of the afterglow.

Figure 2 shows the projected size expansion of GRB 221009A (blue symbols) and compares it with the only other GRB 030329 for which such a measurement could be obtained (Taylor et al. 2024).

The size expansion rate measured in GRB 221009A is consistent with that expected from the FS of an ultra-relativistic spherical blast wave (Blandford & McKee 1976). However, in this scenario, if the jet break has not yet happened on the timescales probed by EVN observations it would imply that the jet should have an extremely large kinetic energy. A low external medium density or a structured jet would resolve this demanding large energetic requirement (Gill & Granot 2023).

Giarratana et al. (2024) measured the source size expansion on different frequencies: the 4.9-8.3 GHz frequency range covered by the EVN observations and the 15 GHz by the VLBA. This study highlights, for the first time, a frequency-dependent size evolution with the higher frequencies displaying a faster size expansion rate ($\propto t^{0.98\pm0.36}$ - 15 GHz – versus $\propto t^{0.79\pm0.20}$ – 4.9–8.3 GHz). A possible intriguing interpretation, in agreement with the radio afterglow modelling (e.g. Ren et al. 2023; Laskar et al. (2023)), is that the early lower frequencies

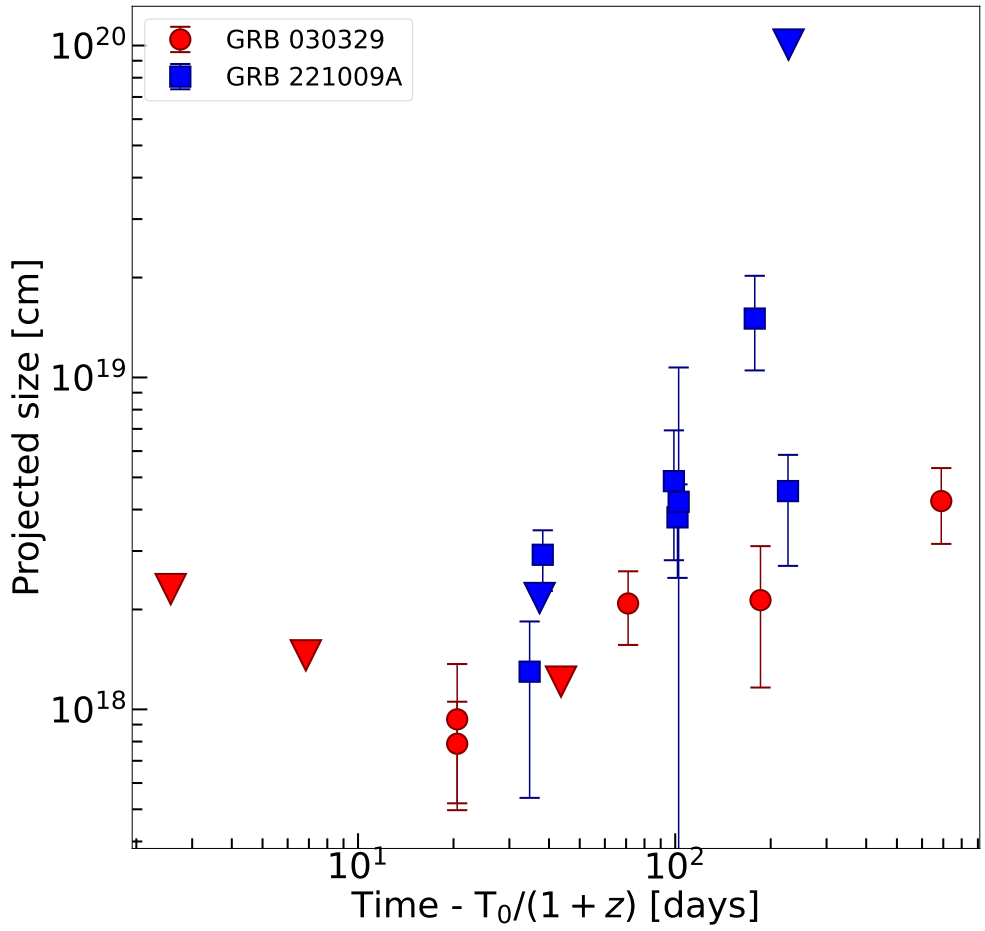

Fig. 2: Projected size versus rest frame time (referenced to the trigger time of the GRB) for GRB 221009A and GRB 030329 (symbols shown in the legend). The data of GRB 030329 are from Taylor et al. 2004. Figure from Giarratana et al. (2024).

radio emission is dominated by the RS while the higher frequency emission is due to the FS.

Another bursts which allowed to exploit the high resolution imaging of VLBI observations is GRB 190829A. This is a relatively low power GRB (with equivalent isotropic energy, $E_{\rm iso} \sim 3 \times 10^{50}$ erg), at ∼370 Mpc from the Earth. It is among the few GRBs detected at TeV energies (de Naurois & H. E. S. S. Collaboration 2019). EVN+e-MERLIN (at 5 GHz) and VLBA (at 15 GHz) observations were obtained distributed between 9 and 117 days after the burst (Salafia et al. 2022). The source is significantly detected in all observations but remains unresolved on the scales of the few milliarseconds resolution reached. Through a Markov Chain Monte Carlo method the source size upper limits were obtained. These are shown by the down arrows in Fig. 3 (central panel). The three EVN epochs images are also shown in Fig. 3 (upper panels). Semi-analytical models (Granot et al. 1999, Salafia et al. 2022 - dotted line and shaded curves in Fig. 3) predict that the observed size s expansion of a relativistic jet observed close to its axis should scale as $s \propto l^{3/8} t^{5/8}$ where l is the Sedov lenght, namely a function of the ratio between the jet energy and the circum-burst medium. These are also among the leading parameters determining the afterglow multi–wavelength emission from the radio to the TeV energy range. Therefore by combining the modelling of the afterglow light curve (see Fig.3 in Salafia et al. 2022) with the constraints on the Sedov length from radio VLBI observations, it was possible to show that in GRB 190829A only a relatively low fraction (<1%) of electrons are accelerated into a non-thermal energy distribution at the shock front and are responsible for the afterglow emission. Moreover, the resulting low magnetic field energy density (in line with other GRB results - e.g. Barniol Duran 2014) points to an inefficient magnetic amplification by turbulence at the shock front or a fast magnetic field decay behind it. One key result is that the high-energy TeV emissions observed by HESS are most likely caused by synchrotron self-Compton processes within the forward shock. Although the constraints from VLBI data make it unlikely that the GRB was viewed off-axis, the possibility cannot be ruled out entirely and would require an angle within 2° of the jet edge.

4. The role of radio observations in multi-messenger astronomy

The VLBI imaging of the afterglow of GRB 170817 eventually probed the presence of a relativistic jet which succesfully emerged from the dense environment shed apart by the merger of the neutron stars responsible for the gravitational wave signal GW170817. Indeed, the slow rise ($\propto t^{+0.8}$) and late peak (150 days post burst -

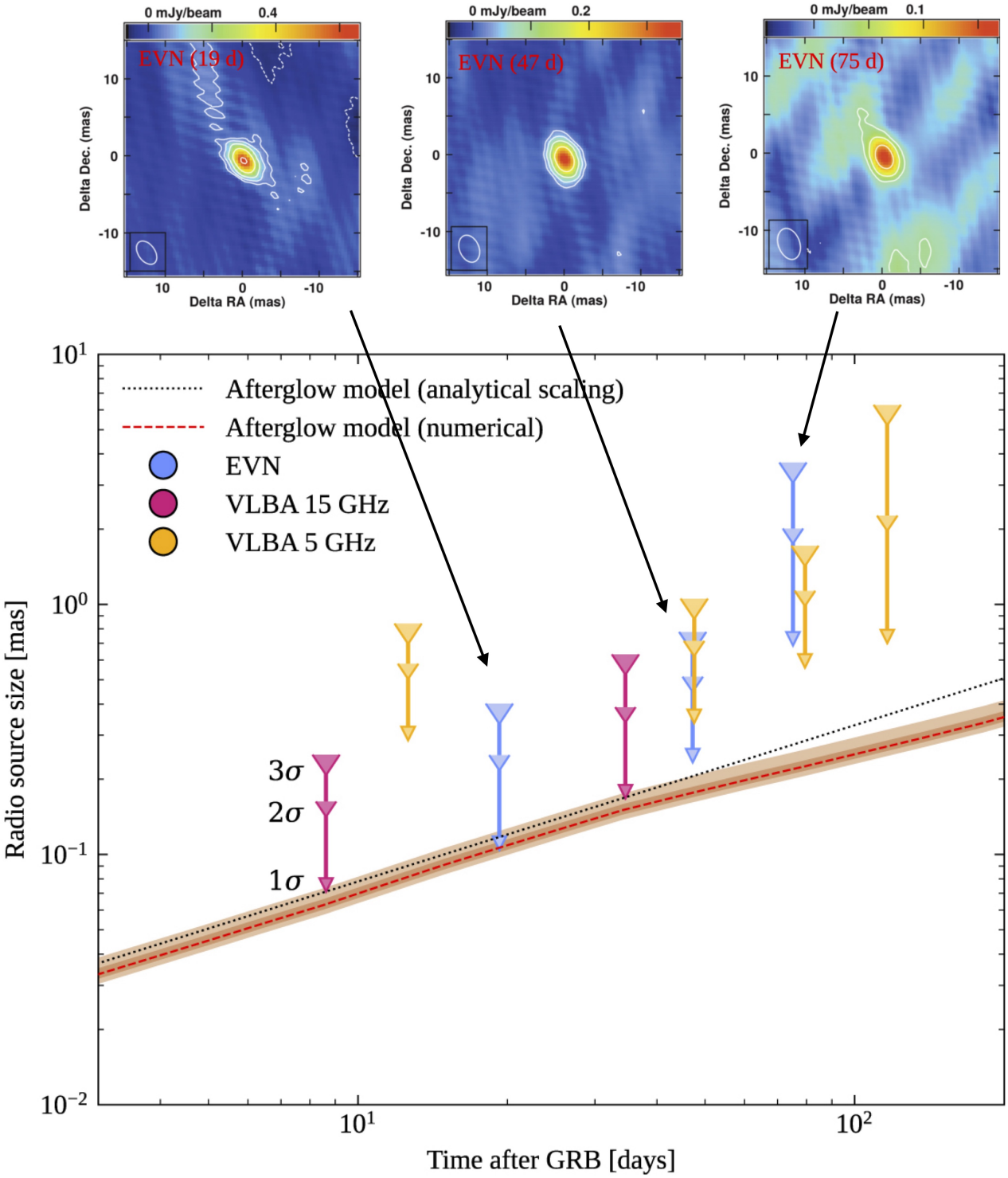

Fig. 3: Constraints (1,2 and 3σ upper limits) on the prohected size of the blast wave of GRB 190829A versus time obtained thorugh EVN and VLBA observations (as labelled). The three EVN epochs images are also shown in the top panel along with arrows correpsonding to the infferred limits. Adapted from Salafia et al. 2022.

D'Avanzo et al. 2018) of the multiwavelenght afterglow light curve could be interpreted as due to a nearly spherical outflow with a radially stratified velocity distribution or with an angularly structured jet (in both energy and bulk velocity) observed at large angles. The measurement of the proper motion of the source (Mooley et al. 2018) and the constrain on the source size < 2.5 mas at 170 days (Ghirlanda et al. 2019) when combined with the multi-

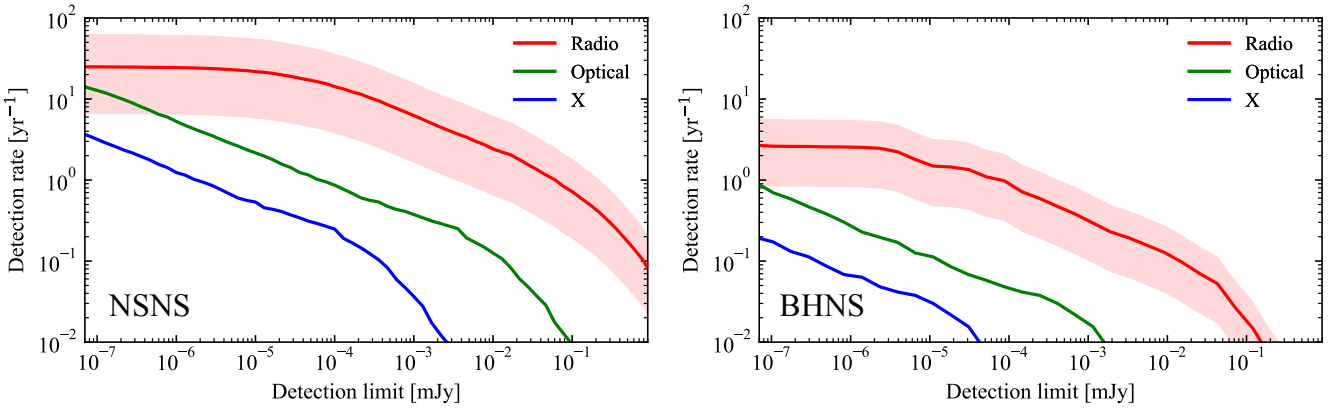

Fig. 4: Detection rate of the afterglow counterparts of gravitational wave events detectable during the 5th run of the Ligo-Virgo-Kagra intreferometers (Colombo et al. 2022; Colombo et al. 2024).

wavelength afterglow modelling suggested that a structured jet with a narrow core and a powerlaw angularly distributed energy could account for most observational evidences if observed at ∼20 degrees off axis. The combined EM and GW analysis could break the angle distance degeneracy proper of the GW signal.

Despite the lack of any additional mult-messenger event after 170817 as of now, the prospects for the detection of binaries with two neutron stars (BNS) or a neurtron star and a black hole (BHNS) during the upgraded runs of the Ligo-Virgo-Kagra (LVK) ground based detectors are promising[1]. During the fifth observing run, expected to start in 2028, an estimated number of 180^{+220}_{-100} BNS and 30^{+42}_{-20} BHNS per year are expected within a median redshift 0.15 and 0.3 respectively.

Owing to the common depedence of the GW and EM signal on the source orientation, namely being louder and brighter, respectively, the more on oaxis (or face on) the system is oriented, off axis events will dominate the detections in the local Universe while at larger distances only more on-axis cases will be preferentially detected.

Predictions of the expected joint (GW+EM) detection rates during the future runs of the current GW detectors or in the era of the third generation detectors are based on population synthesis models. In a seried of works, Colombo et al. (2022, 2024) built a population synthesis model which includes the modelling of the GW signal from a population of binaries (either BHNS and NSNS) and the associated EM emission componenets, namely the Kilonova and GRB emission.

As an example of these predictions, Fig. 4 shows the cumulative detection rate of BNS (left panel) and BHNS (right panel) distribution as a function of the afterglow emission in the radio, optical and X–ray for the GW events detectable by LVK during the fifth observing run (O5). In particular the radio flux density is computed at 1.4 GHz. The radio emission is the brightest and it represents the optimal band for the sarch and follow up of the EM counterparts of GW sources.

[1] https://emfollow.docs.ligo.org/userguide/capabilities.html

One possible EM signal from BNS and BHNS which is expected from purely theoretical grounds but has not been clearly detected in 170817, is the kilonova afterglow. The ultra-relativistic jet launched by the central engine should expand ahead of the mildly relativistic more isotropic merger ejecta. Moreover, owing to its deceleration, the jet should also start to expand sideways while propagating into the circum-burst medium. In this expansion it should sweep up the ISM material creating an ideally quasi spherical cavity whose border can be thought as an overdensity shell. When the isotropic mildly relativistic ejecta, responsible for the KN emission, eventually reach this over-density region they should produce an afterglow (so called KN afterglow). The timescales of this process are quite long (e.g. Margalit & Piran 2020) ∼ a few years post merger. Such a long timescale signal could be best detected in the radio band. If so it would probe the dynamics of the merger ejecta.

Acknowledgements. S.Giarratana, O. S. Salafia, M. Giroletti are acknowledged for the continuous and stimulating collaboration. GG acknowledges INAF Grant 1.05.23.06.04 (POEMS) and the European Union-Next Generation EU, PRIN 2022 RFF M4C21.1 (202298J7KT - PEACE).

References

Abbott, B. P., Abbott, R., Abbott, T. D., et al. 2017, ApJ, 848, L12
Barniol Duran, R. 2014, MNRAS, 442, 3147
Berger, E. 2014, ARA&A, 52, 43
Blandford, R. D. & McKee, C. F. 1976, Physics of Fluids, 19, 1130
Bright, J. S., Rhodes, L., Farah, W., et al. 2023, Nature Astronomy, 7, 986
Chandra, P. & Frail, D. A. 2012, ApJ, 746, 156
Colombo, A., Salafia, O. S., Gabrielli, F., et al. 2022, ApJ, 937, 79
Colombo, A., Duqué, R., Salafia, O. S., et al. 2024, A&A, 686, A265
Cucchiara, A., Levan, A. J., Fox, D. B., et al. 2011, ApJ, 736, 7

D'Avanzo, P., Campana, S., Salafia, O. S., et al. 2018, A&A, 613, L1
de Naurois, M. & H. E. S. S. Collaboration 2019, GRB Coordinates Network, Circular Service, No. 25566, 25566
Gehrels, N., Chincarini, G., Giommi, P., et al. 2004, ApJ, 611, 1005
Ghirlanda, G., Salvaterra, R., Burlon, D., et al. 2013, MNRAS, 435, 2543
Ghirlanda, G., Salafia, O. S., Paragi, Z., et al. 2019, Science, 363, 968
Giarratana, S., Salafia, O. S., Giroletti, M., et al. 2024, A&A, 690, A74
Gill, R. & Granot, J. 2023, MNRAS, 524, L78
Granot, J., Piran, T., & Sari, R. 1999, A&AS, 138, 541
Laskar, T., Alexander, K. D., Margutti, R., et al. 2023, ApJ, 946, L23
Margalit, B. & Piran, T. 2020, MNRAS, 495, 4981
Mooley, K. P., Nakar, E., Hotokezaka, K., et al. 2018, Nature, 554, 207
Perley, D. A., Cenko, S. B., Corsi, A., et al. 2014, ApJ, 781, 37
Ren, J., Wang, Y., Zhang, L.-L., et al. 2023, ApJ, 947, 53
Salafia, O. S., Ravasio, M. E., Yang, J., et al. 2022, ApJ, 931, L19
Taylor, G. B., Frail, D. A., Berger, E., et al. 2004, ApJ, 609, L1